Article ID: 1000-7032(2024)01-0139-10

Narrowband 1 550 nm Photodetection Based on Plasmon-enhanced Upconversion Luminescence

ZHOU Boming, QIN Zisheng, WANG Shuhuan, YANG Zongyuan, JIANG Weiyao, ZHAO Heran, CAO Peng, BAO Minjie, CHENG Huining, JI Yanan*

(*Key Laboratory of New Energy and Rare Earth Resource Utilization of State Ethnic Affairs Commission, Key Laboratory of Photosensitive Materials & Devices of Liaoning Province, School of Physics and Materials Engineering, Dalian Minzu University, Dalian* 116600, *China*)

* *Corresponding Author, E-mail: jiyn@dlnu.edu.cn*

Abstract: Near-infrared (NIR) detection technology plays an important role in military, communications and industrial applications. The huge market demand has led to a rapid development of research in NIR photodetectors (PDs). Rare earth doped upconversion nanoparticles (UCNPs) with two- or multi-photon pumping characteristics can convert NIR photons to visible or ultra-violet photons and be absorbed by semiconductors with wider bandgaps, producing upconversion PDs with excellent performance. However, the implementation of NIR narrowband upconversion PDs still faces several difficulties, such as rare earth ion fluorescence quantum low efficiency, and the need for high pumping thresholds to achieve detectable upconversion luminescence. Herein, we utilized $NaYF_4$:4%Er UCNPs combined with perovskite semiconductor layers to achieve a narrowband upconversion PDs of 1 550 nm. Upconversion luminescence of UCNPs is enhanced by using Ag nanorods (NRs) layers with localized surface plasmon resonance effect, thus lowing the pump threshold of the upconversion PDs. The optimized responsivity (R) and detectivity (D^*) of Ag NRs/$NaYF_4$:4%Er UCNPs/$MAPbI_3$ hybrid upconversion PDs are ~48.5 mA/W and 5.7×10^8 Jones, respectively. Compared with the pure UNCPs/$MAPbI_3$ upconversion PDs, both the R and D^* of hybrids PDs have improved by an order of magnitude. We have successfully constructed a simple strategy to make stable NIR narrowband PDs.

Key words: upconversion luminescence; localized surface plasmon resonance; local field modulation; narrowband near-infrared photodetectors

CLC number: TN215 **Document code**: A **DOI**: 10.37188/CJL.20230248

基于等离子体增强上转换发光的窄带 1 550 nm 光探测

周博明，覃子晟，王姝欢，杨棕媛，江苇瑶，赵赫然，
曹 鹏，鲍民杰，程惠宁，季亚楠*

（大连民族大学 物理与材料工程学院，国家民委新能源与稀土资源利用重点实验室，
辽宁省光敏材料与器件重点实验室，辽宁 大连 116600）

摘要：近红外光(NIR)探测技术在军事、通信和工业应用中发挥着重要的作用，巨大的市场需求带动了NIR光电探测器(PDs)研究的快速发展。具有双光子或多光子泵浦特性的稀土掺杂上转换纳米颗粒(UCNPs)可以

收稿日期：2023-10-24；**修订日期**：2023-11-07
基金项目：国家自然科学基金(12104084)；辽宁省教育厅基本科研项目(LJKQR20222484)；大连市科技人才创新支持政策(2022RQ020)；区域光纤通信网与新型光通信系统国家重点实验室开放基金(2023GZKF06)
Supported by National Natural Science Foundation of China(12104084); Basic Scientific Research Project of Education Department of Liaoning Province(LJKQZ20222455); Science and Technology Talent Innovation Support Policy Project of Dalian(2022RQ020); State Key Laboratory of Advanced Optical Communication Systems and Networks(2023GZKF06)

将NIR光子转换为可见光子或紫外光子，并被禁带宽度更宽的半导体吸收，进而制备出性能优异的上转换PDs。然而，NIR窄带上转换PDs的实现仍然面临一些困难，例如稀土离子荧光量子效率低、需要高泵浦阈值才能实现可探测的上转换发光。在此，我们利用$NaYF_4$:4%Er UCNPs与钙钛矿半导体层相结合，实现了1 550 nm的窄带上转换PDs。通过使用具有局域表面等离子体共振效应的银纳米棒层(Ag NRs)增强了UCNPs的上转换发光，从而降低了上转换PDs的泵浦阈值。基于Ag NRs/$NaYF_4$:4%Er UCNPs/$MAPbI_3$复合结构的PDs的最佳响应度(R)和探测率(D^*)分别约为48.5 mA/W和5.7×10^8 Jones。与纯UNCP/$MAPbI_3$ PDs相比，R和D^*均提高了一个数量级。我们成功地构建了一种简单的策略来制造出稳定的近红外窄带PDs。

关 键 词：上转换发光；局域表面等离子体共振；局域场调制；窄带近红外光电探测器

1 Introduction

In recent decades, photodetectors (PDs) have developed rapidly and have been widely used in our daily life. The narrowband near-infrared (NIR) PDs have great development potential in many industrial fields including remote light detection, optoelectronics, satellite maps and medical devices[1-2]. Especially for photodetection at 1 550 nm wavelength, which is crucial to industrial imaging applications and military, such as laser-beam profile inspection, visualization of military targeting lasers, and night vision[3-5]. However, the majority of PDs are non-selective and are operated over a broad range of wavelengths determined by the bandgap of the photoactive materials[6-7]. There are lots of emerging materials have been developed for narrowband NIR detection over recent decades, for example, quantum dots, two-dimensional semiconductor materials[8-10]. Moreover, using an external optical bandpass filter/optical microcavity couple with broadband devices or charge collection narrowing conception can also obtain narrowband PDs[11]. Though these materials demonstrate pretty high electronic mobility as well as consume low power, and the above mentioned strategies are also proved to be effective, they are not suitable for next-generation electronic devices in further applications due to their limitations of complexity, high cost, and strictly controlled manufacturing process[12-13]. For example, some conventional semiconductor compounds such as $In_xGa_{1-x}As$, Si and HgTe, *etc*. These materials have encountered a bottleneck in modern electronics and photonics in terms of spectral coverage, low resolution, non-transparency, inflexible, and complementary metal-oxide-semiconductor incompatibility[14-15]. Though the maturity of InGaAs-based NIR PDs technologies, there are still some major roadblocks for large-scale deployment.

Lanthanide-doped upconversion nanoparticles (UCNPs) are generally considered as the most effective NIR absorption materials, which can convert photons in low-energy states to those in the high-energy states, thereafter easily detect NIR light up to wavelength of 1 550 nm[16-17]. Owing to the narrow absorbance of rare earth ions in NIR range, the full-widths at half maximum of UCNPs-based PDs' are usually below 30 nm[4,18]. Apart from that, the UCNPs-based PDs are also suitable for transparent and flexible optoelectronic devices[19]. But the UCNPs usually have low quantum yields, hence some efficient auxiliary strategies have been commonly used to improve the upconversion luminescence (UCL) intensities, such as core-shell design[20], photonic crystal effect[21], as well as introduction of localized surface plasmon resonance (LSPR) effect[22]. Especially, the LSPR effect can significantly boost the excitation rate and emission efficiency of UCNPs due to the local field amplification in the proximity of noble metal nanostructures (like Au, Ag, or Pt) in the plasmonic modulation of UC emission[23-24]. In the reported works of PDs based on the UCNPs hitherto, most focus on detection at wavelength of 980 nm[18,25-26]. Considering these advantages the above mentioned, it is necessary to combine UCNPs with semiconductor materials to enable devices to achieve NIR narrowband photodetection at 1 550 nm.

In this work, we selected noble metal Ag nanorods (NRs) as plasmonic architecture and synthesized

$NaYF_4$: 4%Er UCNPs, thereafter fabricated the Ag NRs/$NaYF_4$: 4%Er UCNPs as hybrid plasmonic UC films. As a result, we obtained ~13 folds of UCL intensities enhancement. Thereafter, the narrowband 1 550 nm PDs were developed based on $MAPbI_3$/Ag NRs/UCNPs composites, the responsivity (R) and detectivity (D^*) are ~48.5 mA/W and 5.7×10^8 Jones, respectively.

2 Experimental

2.1 Chemicals and Materials

Hexadecyl trimethyl ammonium bromide (CTAB), ascorbic acid (AA), cetyltrime-thylammonium chloride (CTAC, 97%), polyvinyl pyrrolidone (PVP), sodium borohydride ($NaBH_4$), sodium oleate (NaOL), sliver nitrate ($AgNO_3$), and chloroauric acid ($HAuCl_4$), deionized water. Yttrium (Ⅲ) acetate hydrate ($Y(CH_3CO_2)_3$, 99.9%), erbium (Ⅲ) acetate hydrate ($Er(CH_3CO_2)_3$, 99.9%), sodium hydroxide (NaOH, ≥98%), ammonium fluoride (NH_4F, ≥98%), oleic acid (OA, 90%), 1-octadecence (ODE, 90%), cyclohexane (99.5%), absolute alcohol. Dimethyl sulfoxide (DMSO), N, N-dimethylformamide (DMF, ≥99%), PbI_2 (99.9%), Methylammonium iodide (MAI, ≥99.5%), chlorobenzene. Unless otherwise noted, all the chemicals were used without further purification.

2.2 Synthesis of Ag NRs

The Ag NRs were obtained by a typical seeded growth method[27]. The first part: CTAB (5 mL, 0.2 mol·L^{-1}) was mixed with $HAuCl_4$ (5 mL, 0.5 mmol·L^{-1}). A freshly prepared $NaBH_4$ solution (0.6 mL, 0.01 mol·L^{-1}) was diluted to 1 mL then added to the above mixture solution under the vigorous agitation. After stirring for 3 min, the color of solution changed from yellow to light brown, and aged for 30 min to be used as seed liquid. The second part: 0.025 g NaOL was dissolved in 5 mL deionized water, and reacted with 0.137 g CTAB at 50 ℃. After the temperature cooled down to 30 ℃, added 18 μL $AgNO_3$ solution (0.1 mol·L^{-1}) into the above mixtures and let stand for 15 min. Then added $HAuCl_4$ solution (5 mL, 1 mmol·L^{-1}) to the above solution, kept stirring until the solution becomes colorless. At this point, 72 μL of HCl (37% in water 12.1 mol·L^{-1}) was needed to adjust pH of the solution. After stirring for 15 min, added AA (1.25 mL, 64 mmol·L^{-1}) solution and kept vigorously stir for 30 s and used as a growth solution. The third part: added 125 μL seed solution to 10 mL growth solution, and kept stirring for 30 s, after that let it stand 12 h at room temperature. The final product were isolated and washed by centrifugation with deionized water.

2.3 Synthesis of $NaYF_4$:4%Er UCNPs

We used solvothermal method to prepare the UCNPs[28]. A mixture of 3 mL OA, 7 mL ODE, and 2 mL aqueous solution containing a total amount of 0.4 mmol lanthanide ($Y(CH_3CO_2)_3$ and $Er(CH_3CO_2)_3$) with 24∶1 ratios were added into a 50-mL three-necked flask. The mixture was heated at 150 ℃ for 1 h and then cooled to 30 ℃. Then 6 mL methanol solution containing 1 mmol NaOH and 1.6 mmol NH_4F was added and stirred at 50 ℃ for 45 min. After that the methanol was evaporated at 100 ℃ for 1 h. Subsequently, the reaction solution was then heated to 300 ℃ for 1.5 h under nitrogen atmosphere. The product was collected by centrifugation, and washed with ethanol for three times, and finally re-dispersed in 5 mL of cyclohexane.

2.4 Fabrication of Ag NRs/UCNPs Hybrids

Herein, we used three-phase self-assembly method to fabricate monolayer Ag NRs and UCNPs films to obtain Ag N Rs/UCNPs hybrid structures[28-29]. The precipitate of Ag NRs (UCNPs, the following is omitted) were dispersed in dilute HCl (10 mL, 1 mol·L^{-1}) and amply dissolved by ultrasonic. The mixture was centrifuged to remove the excess OA ligands, then dispersed in the ethanol solution of PVP (1%, wt/v) again. Repeat last operation, and the PVP-coated Ag NRs were prepared. The CH_2Cl_2 (800 μL), deionized water (1.8 mL) and PVP-coated Ag NRs solution (50 μL) were subsequently added into an reaction bottle with vigorously shaking for 30 s. Then n-hexane (6 mL) was added into the above mixture. Thereafter, the Ag NRs can be driven to the upper interface of the deionized water and n-hexane phase. Finally, the monolayer Ag NRs

film was successfully transferred onto a glass substrate(1 cm×1 cm) by dip-coating method.

2.5 Fabrication of UCNPs/MAPbI$_3$ and Ag NRs/UCNPs/MAPbI$_3$ PDs

The MAI and PbI_2 were mixed in DMSO solution to prepare the perovskite precursor. The perovskite films were fabricated on the UCNPs glass substrate by utilized two-step method at the nitrogen atmosphere. Notably, the chlorobenzene (100 μL) was kept on the spinning substrate for ~20 s prior to the end of the spinning program during the second step. Then the $MAPbI_3$ films need to be annealed at 100 ℃ for 10 min. Finally, approximately 100 nm Ag electrodes deposited onto the $MAPbI_3$ layers *via* thermal evaporation.

2.6 Measurement and Characterization

All characterizations about the morphology as well as phase structures were separately measured by transmission electron microscope (Hitachi H-8100IV, Japan) and X-ray diffraction (XRD). The absorption spectra were obtained by ultraviolet(UV)/visible (Vis)-NIR scanning spectrophotometer instrument(Shimadzu UV-3600PC, Japan). The emission spectrum and luminescence kinetics data were acquired by the spectrometer(Horiba, Japan), Edinburgh instruments FLS1000, and digital phosphor oscilloscopes(Tektronix DPO5104, America), respectively. All the photodetection performance tests of UCNPs/$MAPbI_3$ hybrids and Ag NRs/UCNPs/$MAPbI_3$ PDs were gained by sourcemeter(Keithley 2400, America).

3 Results and Discussion

We prepared $NaYF_4$:4%Er UCNPs by using the solvent thermal method, and their transmission electron microscopy(TEM) image in Fig.1(a) shows that the UCNPs are homogeneous and monodispersed with a diameter of (23.2±1.5) nm. The XRD pattern of UCNPs films is displayed in Fig. 1(b), which is greatly consistent with the standard card of β-$NaYF_4$ (PDF 16-0344). Noble metal nanorods have been the focus of lots of recent researches due to their potential use as active components or interconnects in fabricating electronic, photonic, and solar cells, *et al*[30]. Compared with Au NRs, Ag NRs have controllable aspect ratios, high purity, and high dimensional uniformity[31]. Ag NRs seem to be particularly

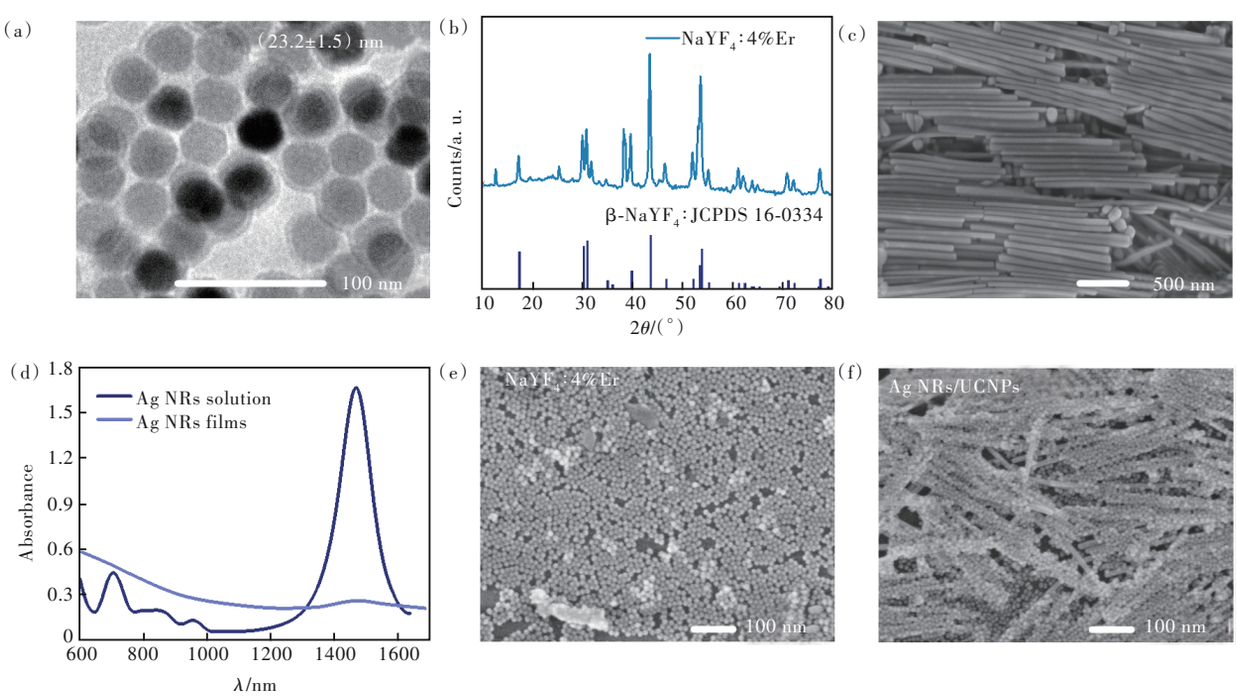

Fig.1 (a)The TEM image of $NaYF_4$:4%Er UCNPs, the inset is the particle size distribution of UCNPs. (b)The XRD pattern of $NaYF_4$:4%Er UCNPs. (c)The SEM image of Ag NRs. (d)The absorption spectra of pure Ag NRs solution and Ag NRs films. The top-view of SEM images of $NaYF_4$:4%Er films(e) and Ag NRs/$NaYF_4$:4%Er hybrids(f), respectively

worthy of synthesis and study, as bulk silver shows the highest electrical and thermal conductivities of all metals[32-33]. Hence, we have been successfully synthesized Ag NRs through hydrothermal method[27]. Fig. 1(c) displays the SEM image of some Ag NRs that had a mean diameter of ~(1.45±0.25) μm with 14.5 aspect ratio. The extinction spectra of Ag NRs solution and random aggregated Ag NRs films were shown in Fig. 1(d). The longitudinal absorption peak after Ag NRs deposition becomes broadened, which can be attributed to the absorption of SPR around 1 550 nm. Hereafter, UCNPs were further assembled on the glass substrate through spin-coated method, and the Ag NRs/UCNPs hybrid films were fabricated by also using the aforementioned route. Their top-view SEM image was exhibited in Fig. 1(e) and 1(f), respectively.

In Fig. 2(a), UC energy level diagram of β-$NaYF_4$:4%Er UCNPs excited at 1 550 nm, and Er^{3+} can absorb multiple photons at NIR region with narrowband absorption thereafter emit photons at higher energies in the Vis range. Correspondingly, the UCL spectra of UNCPs and Ag NRs/UCNPs hybrids are shown in Fig. 2(b). The classic green and red UC emissions of Er^{3+} ions in both of the UCNPs and Ag NRs/UCNPs hybrids samples are observed. To be brief, Er^{3+} ions were pumped by 1 550 nm excitation light and then generated green emission at 525/545 nm ($^2H_{11/2}/^4S_{3/2}\rightarrow{}^4I_{15/2}$) and red emission at 656 nm ($^4F_{9/2}\rightarrow{}^4I_{15/2}$) through energy transfer and/or multiple excited state absorption processes. And the UCL intensities of UCNPs in Ag NRs/UCNPs hybrids are significantly enhanced by a factor of approximately 12.65. The power-dependent UCL intensity of the $^2H_{11/2}$, $^4S_{3/2}\rightarrow{}^4I_{15/2}$ and $^4F_{9/2}\rightarrow{}^4I_{15/2}$ emission transitions in pure UCNPs and Ag NRs/UCNPs hybrids is exhibited in Fig. 2(c). From the In-In plot ($I_{UCL}\propto P^n$), slopes n for the $^2H_{11/2}$, $^4S_{3/2}\rightarrow{}^4I_{15/2}$ and $^4F_{9/2}\rightarrow{}^4I_{15/2}$ emissions in the above two kinds samples are separately close to 3, the photon number required to populate the $^2H_{11/2}$, $^4S_{3/2}$ and $^4F_{9/2}$ levels for all of the samples. Such n values indicates that the emissions at 525/545 nm and 656 nm were three-step UC($2<n<3$)[34]. In addition, for further understanding the UCL enhancement behaviour coupling with Ag NRs films, we investigated the UCL dynamic of Er^{3+} emissions under the 1 550 nm excitation, as shown in Fig. 3(a)-(b). It can be seen that the change for the $^4S_{3/2}\rightarrow{}^4I_{15/2}$ and $^4F_{9/2}\rightarrow{}^4I_{15/2}$ of Er^{3+} decay times for UCNPs as well as Ag NRs/UCNPs hybrids is less than 15%. This result is consistent with previous works, and it can be deduced that the UCL enhancement comes mainly from the interaction of Ag NRs with excitation electric field, rather than the interaction with emission electric field[35].

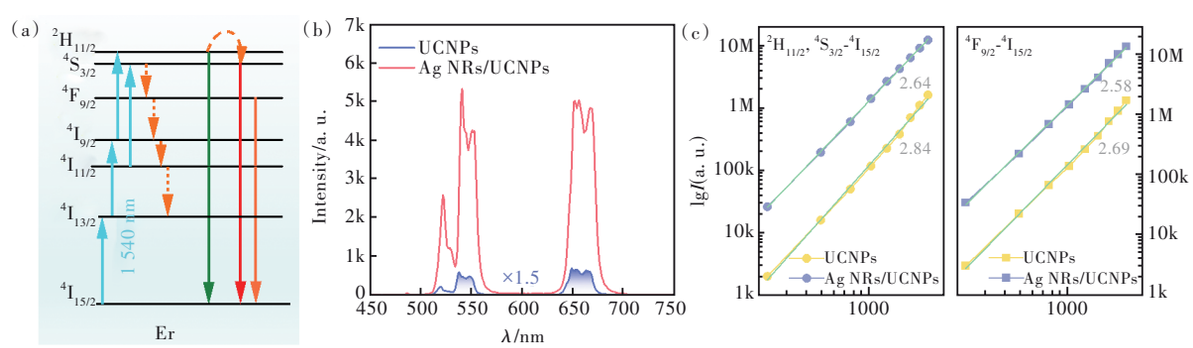

Fig.2　(a) The upconversion energy level diagram of β-$NaYF_4$:4%Er UCNPs excited at 1 550 nm. (b) The upconversion emission of Er^{3+} ions under illumination at 1 550 nm of pure UCNPs and Ag NRs/UCNPs hybrids, respectively. (c) The power-dependent UCL intensity of the $^4S_{3/2}/^2H_{11/2}$-$^4I_{15/2}$ (left panel) and $^4F_{9/2}\rightarrow{}^4I_{15/2}$ (right panel) emission transitions in pure UCNPs and Ag NRs/UCNPs hybrids

Encouraged by the advantages of UCNPs in optoelectronic devices, on the basis of enhancing UCL with Ag NRs, we fabricated narrowband NIR PDs. The PDs were composed of Ag NRs/UCNPs hybrid films, high-quality perovskite semiconductor ($MAPbI_3$) layers, and silver electrodes are top of them,

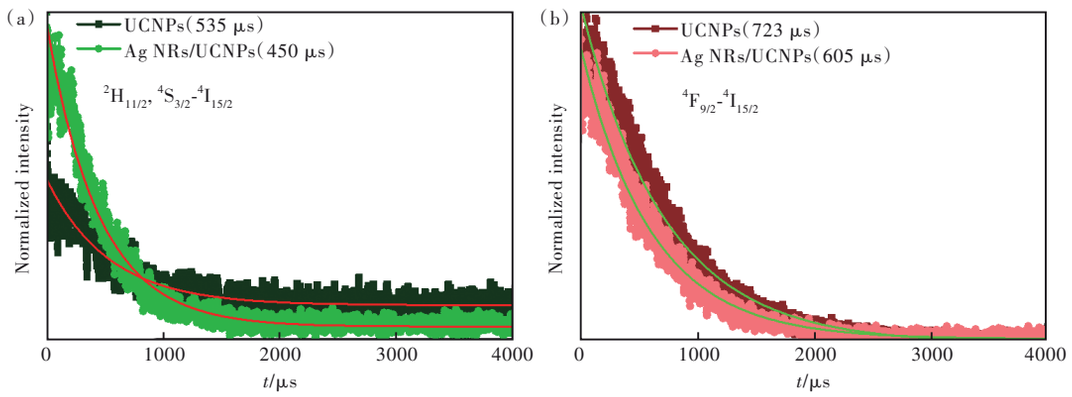

Fig.3 The luminescence dynamics of $^4S_{3/2}/^2H_{11/2}$-$^4I_{15/2}$ (a) and $^4F_{9/2}$-$^4I_{15/2}$ (b) emissions in pure UCNPs and Ag NRs/UCNPs hybrids at 1 550 nm excitation

as shown in Fig. 4(a)(left). The working mechanism of the devices is depicted in Fig. 4(a)(right), the $NaYF_4$: 4%Er UCNPs can be excited by 1 550 nm light and emit visible light in the spectral range of 500–700 nm through photon upconversion processes. The $MAPbI_3$ layers can absorb the lights in the region from 300–750 nm, therefore the upconverted light can be absorbed by the $MAPbI_3$ layers thereby producing photocurrents under the action of bias voltage. The normalized emission and absorption spectra of UCNPs and $MAPbI_3$ are shown in Fig. 4(b), and the illustration is the top-view SEM picture of the $MAPbI_3$ layers. Subsequently, the photoresponse properties of these UCNPs based PDs

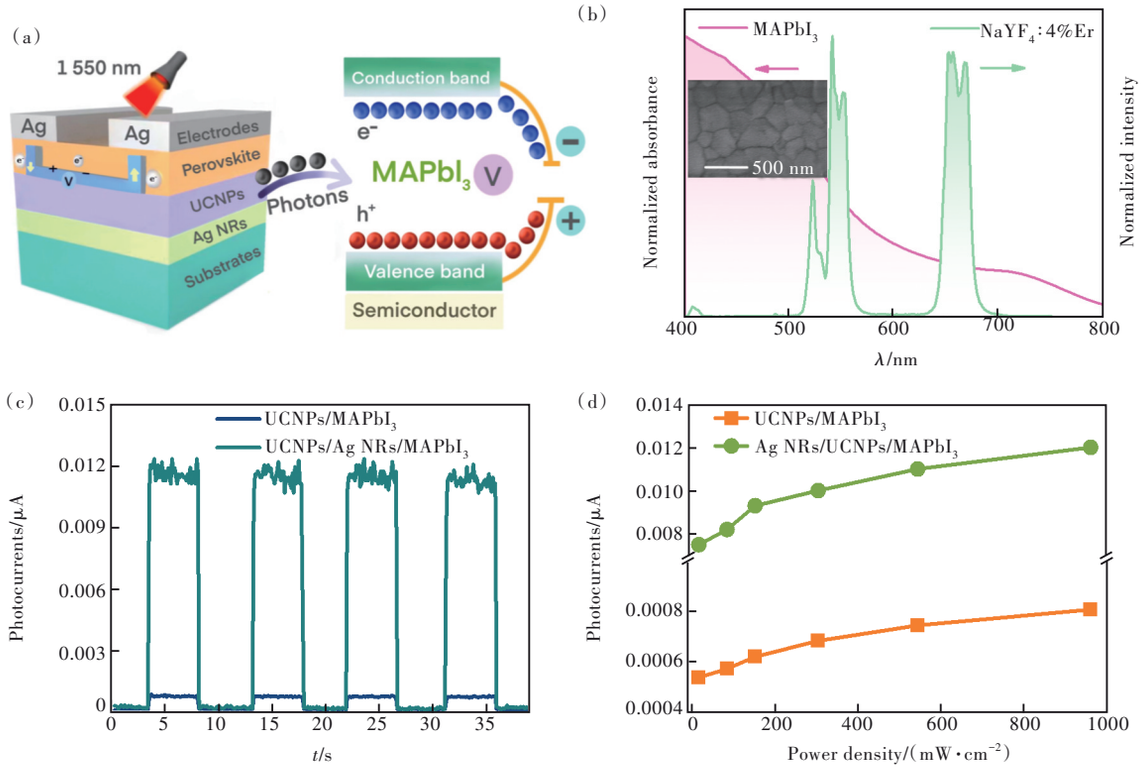

Fig.4 (a) Schematic illustration of the structure and device's mechanism of NIR narrowband PDs at 1 550 nm based on the Ag NRs/UCNPs/$MAPbI_3$ hybrids. (b) The absorpion of $MAPbI_3$ layers and emission spectra from $^4S_{3/2}/^2H_{11/2}$-$^4I_{15/2}$ and $^4F_{9/2}\rightarrow{}^4I_{15/2}$ in Ag NRs/UCNPs. The inset is the top-view SEM picture of the $MAPbI_3$ layers. (c) On-off photocurrents of UCNPs/$MAPbI_3$ and Ag NRs/UCNPs/$MAPbI_3$ PDs under 1 550 nm excitation at a power density of 2 mW·cm^{-2}. (d) The reponse photocurrents of the UCNPs/$MAPbI_3$ and Ag NRs/UCNPs/$MAPbI_3$ PDs upon changing the excitation power densities from 15 mW·cm^{-2} to 960 W·cm^{-2}

were characterized. Fig. 4(c) shows the on/off photocurrent-time (*I-t*) response curves of the devices obtained from the UCNPs/$MAPbI_3$ as well as Ag NRs/UCNPs/$MAPbI_3$ PDs under the 1 550 nm illumination. The photocurrents reached 0.001 μA in pristine UCNPs/$MAPbI_3$ PDs and 0.012 μA in Ag NRs/UCNPs/$MAPbI_3$ PDs under the same illumination power densities(2 mW/cm^2). The photocurrents of Ag NRs/UCNPs/$MAPbI_3$ PDs were greatly improved compared with the pristine UCNPs/$MAPbI_3$ PDs, and the amplification factors of photocurrents were estimated to be ~12 folds for 1 550 nm illumination, which corresponds to the UCL enhancement in Fig. 4(c). The photocurrents response under excitation of different laser powers was shown in Fig. 4(d).

We can see that the photocurrents of UCNPs/$MAPbI_3$ and Ag NRs/UCNPs/$MAPbI_3$ PDs increase with the laser power density. We further investigated the responsivity (R), detectivity (D^*), and external quantum efficiency (EQE) of the devices as a function of input illumination power, as exhibited in Fig. 5(a)-(c). R, D^* and EQE(η_{EQE}) satisfy the following equations, respectively:

$$R = \frac{I_{light} - I_{dark}}{PS}, \tag{1}$$

$$D^* = \frac{R}{(2eI_{dark}/S)^{\frac{1}{2}}}, \tag{2}$$

$$\eta_{EQE} = R\frac{hc}{\lambda e}, \tag{3}$$

I_{light} and I_{dark} separately represent the photocurrents of photodetection devices under the illumination and dark environment; P and S separately represent the illumination power density and effective illuminated area; λ is the wavelength of incident light (1 550 nm); h, c and e represent the Planck's constant, elementary charge, and the velocity of light, respectively[36]. The R, D^* and EQE of Ag NRs/UCNPs/$MAPbI_3$ PDs can be reached 48.5 mA/W, 5.7×10^8 Jones, and 3.9%, respectively. While for UCNPs/$MAPbI_3$ PDs, these photodetection performance can only separately reached 2.82 mA/W, 0.5 × 10^8 Jones, and 0.23%. The R, D^* and EQE parameters of these two kinds of PDs have similar trend, which decrease with enhancing the illumination power densities. This is owing to

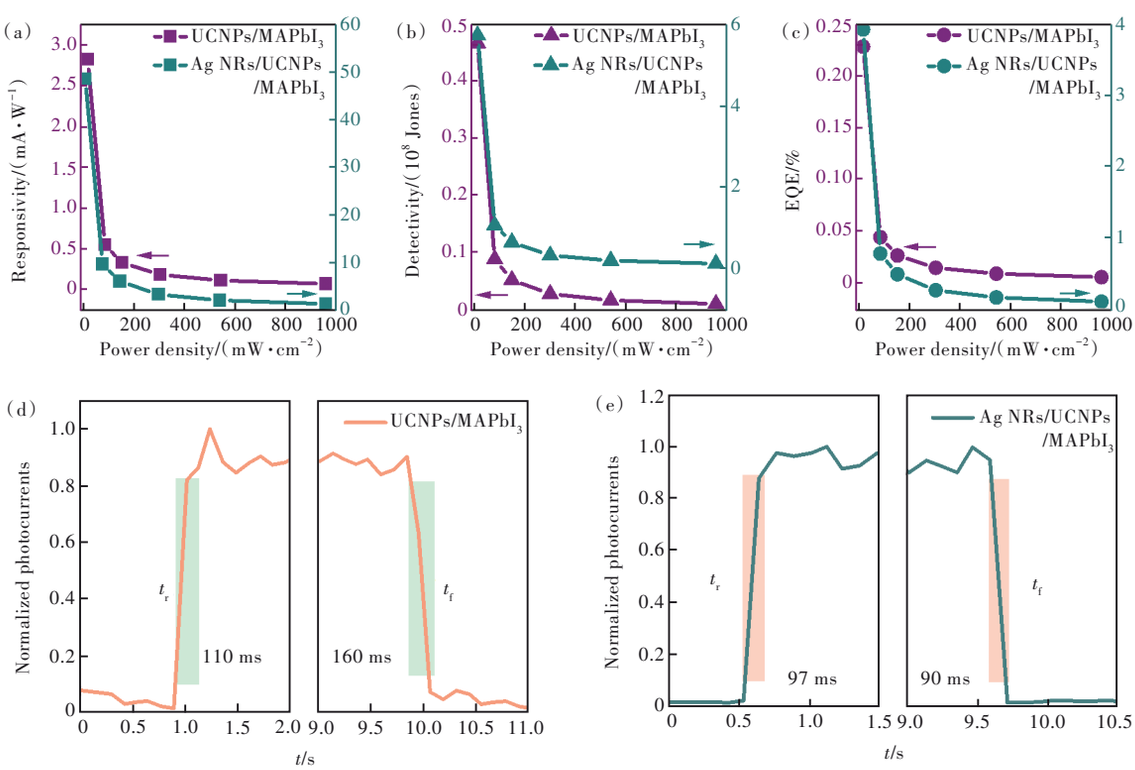

Fig.5　Dependence of the R(a), D^*(b) and EQE(c) of UCNPs/$MAPbI_3$ and Ag NRs/UCNPs/$MAPbI_3$ PDs on the incident light power intensity, respectively. Time-resolved photocurrents of the fabricated UCNPs/$MAPbI_3$(d) and Ag NRs/UCNPs/$MAPbI_3$(e) PDs

the electron-hole recombination loss in $MAPbI_3$ layers, which can be found in previous works. We have achieved approximately 11.4 folds improvement in the photodetection performance of hybrids PDs, which attributed to the LSPR effect of Ag NRs that enhances UC. In Fig. 5(d)-(e), the rising time and falling time of devices are abbreviated as t_r and t_f, respectively. The t_r(t_f) is the time when the photocurrent rises(falls) from 10% to 90%(90% to 10%) of the maximum value after irradiation (turning off light source)[37]. The t_r and t_f of UCNPs/$MAPbI_3$ PDs and Ag NRs/UCNPs/$MAPbI_3$ PDs is ~110 ms and ~97 ms, ~160 ms and ~90 ms, respectively. It can be seen that the introduction of Ag NRs layers has little effect on the response time change of PDs, because of the plasmon induced absorption enhancement of UCNPs rather than the increase of emission rate.

4 Conclusion

In summary, we have demonstrated narrowband 1 550 nm photodetection using Ag NRs/$NaYF_4$:4%Er UCNPs/$MAPbI_3$-based PDs. The UCL can be enhanced by the plasmonic effect of Ag NRs, and correspondingly the response properties of the PDs are significantly improved. Based on this, we obtained good performance of Ag NRs/UCNPs/$MAPbI_3$ PDs, the optimized R and D^* and EQE is ~48.5 mA/W, 5.7×10^8 Jones, and 3.9%, respectively. Although the device photodetection performance is still not as good as that of some advanced two-dimensional materials-based PDs, this would be compensated by the simplicity of fabrication and lower cost of the hybrid UCNPs-based PDs. Overall, the convenient design on UCNPs-based PDs presented in this work provides an alternative approach to realize NIR narrowband photodetection that is not limited to any specific perovskite semiconductor materials.

Response Letter is available for this paper at: http://cjl.lightpublishing.cn/thesisDetails#10.37188/CJL.20230248.

References:

[1] WANG J, XIAO S, QIAN W, *et al*. Self-driven perovskite narrowband photodetectors with tunable spectral responses [J]. *Adv. Mater.*, 2021, 33(3): 2005557.

[2] KUBLITSKI J, FISCHER A, XING S, *et al*. Enhancing sub-bandgap external quantum efficiency by photomultiplication for narrowband organic near-infrared photodetectors [J]. *Nat. Commun.*, 2021, 12(1): 4259.

[3] PECUNIA V. Efficiency and spectral performance of narrowband organic and perovskite photodetectors: a cross-sectional review [J]. *J. Phys. Mater.*, 2019, 2(4): 042001.

[4] JI Y N, XU W, LI D Y, *et al*. Semiconductor plasmon enhanced monolayer upconversion nanoparticles for high performance narrowband near-infrared photodetection [J]. *Nano Energy*, 2019, 61: 211-220.

[5] LIU M, WANG J, ZHAO Z J, *et al*. Ultra-narrow-band NIR photomultiplication organic photodetectors based on charge injection narrowing [J]. *J. Phys. Chem. Lett.*, 2021, 12(11): 2937-2943.

[6] MARTÍNEZ-GOYENECHE L, GIL-ESCRIG L, SUSIC I, *et al*. Narrowband monolithic perovskite-perovskite tandem photodetectors [J]. *Adv. Opt. Mater.*, 2022, 10(22): 2201047.

[7] LI X, GARLISI C, GUAN Q S, *et al*. A review of material aspects in developing direct Z-scheme photocatalysts [J]. *Mater. Today*, 2021, 47: 75-107.

[8] DE ARQUER F P G, ARMIN A, MEREDITH P, *et al*. Solution-processed semiconductors for next-generation photodetectors [J]. *Nat. Rev. Mater.*, 2017, 2(3): 16100.

[9] SHI Y L, WU Z M, DONG X, *et al*. A silicon-based PbSe quantum dot near-infrared photodetector with spectral selectivity [J]. *Nanoscale*, 2021, 13(28): 12306-12313.

[10] LI J Z, WANG J, MA J Q, *et al*. Self-trapped state enabled filterless narrowband photodetections in 2D layered perovskite single crystals [J]. *Nat. Commun.*, 2019, 10(1): 806.

[11] FANG Y J, DONG Q F, SHAO Y C, *et al*. Highly narrowband perovskite single-crystal photodetectors enabled by surface-charge recombination [J]. *Nat. Photonics*, 2015, 9(10): 679-686.

[12] KAN H, ZHENG W, LIN R C, *et al*. Ultrafast photovoltaic-type deep ultraviolet photodetectors using hybrid zero-/two-dimensional heterojunctions [J]. *ACS Appl. Mater. Interfaces*, 2019, 11(8): 8412-8418.

[13] CHOW P C Y, SOMEYA T. Organic photodetectors for next-generation wearable electronics [J]. *Adv. Mater.*, 2020, 32(15): 1902045.

[14] 何嘉玉, 陈克强, 冀婷, 等. 基于二维材料的快速响应金属-半导体-金属结构光电探测器研究进展 [J]. 发光学报, 2022, 43(5): 745-762.
HE J Y, CHEN K Q, JI T, *et al*. Research progress of fast response 2D material photodetectors with metal-semiconductor-metal structure [J]. *Chin. J. Lumin.*, 2022, 43(5): 745-762. (in Chinese)

[15] 苏宛然, 冯琳, 石林林, 等. 表面等离激元增强型光电探测器研究进展 [J]. 发光学报, 2021, 42(7): 1014-1028.
SU W R, FENG L, SHI L L, *et al*. Research progress in surface plasmon enhanced photodetectors [J]. *Chin. J. Lumin.*, 2021, 42(7): 1014-1028. (in Chinese)

[16] JI Y N, FANG G Q, SHANG J Y, *et al*. Aligned plasmonic antenna and upconversion nanoparticles toward polarization-sensitive narrowband photodetection and imaging at 1 550 nm [J]. *ACS Appl. Mater. Interfaces*, 2022, 14(44): 50045-50054.

[17] WEN S H, ZHOU J J, ZHENG K Z, *et al*. Advances in highly doped upconversion nanoparticles [J]. *Nat. Commun.*, 2018, 9(1): 2415.

[18] JI Y N, XU W, DING N, *et al*. Huge upconversion luminescence enhancement by a cascade optical field modulation strategy facilitating selective multispectral narrow-band near-infrared photodetection [J]. *Light Sci. Appl.*, 2020, 9(1): 184.

[19] LEE I, PARK C, KIM T S, *et al*. Water-stable and photo-patternable siloxane-encapsulated upconversion nanoparticles toward flexible near-infrared phototransistors [J]. *Adv. Opt. Mater.*, 2023, 11(12): 2202469.

[20] FAN Y, LIU L, ZHANG F. Exploiting lanthanide-doped upconversion nanoparticles with core/shell structures [J]. *Nano Today*, 2019, 25: 68-84.

[21] JI Y N, XU W, WANG Y, *et al*. Supersensitive sensing based on upconversion nanoparticles through cascade photon amplification at single-particle level [J]. *Sens. Actuators* B *Chem.*, 2022, 367: 132125.

[22] ZHAN Q Q, ZHANG X, ZHAO Y X, *et al*. Tens of thousands-fold upconversion luminescence enhancement induced by a single gold nanorod [J]. *Laser Photon. Rev.*, 2015, 9(5): 479-487.

[23] YANG Y, CONG Y, SHANG J Y, *et al*. NIR LSPR-coupling of Ag nanorices and $W_{18}O_{49}$ nanowires: application of LRET and SERS [J]. *Sens. Actuators* B *Chem.*, 2021, 330: 129199.

[24] LI J, LOU Z Z, LI B J. Engineering plasmonic semiconductors for enhanced photocatalysis [J]. *J. Mater. Chem.* A, 2021, 9(35): 18818-18835.

[25] DING N, XU W, ZHOU D L, *et al*. Upconversion ladder enabled super-sensitive narrowband near-infrared photodetectors based on rare earth doped florine perovskite nanocrystals [J]. *Nano Energy*, 2020, 76: 105103.

[26] LI J B, SHEN Y L, LIU Y C, *et al*. Stable high-performance flexible photodetector based on upconversion nanoparticles/perovskite microarrays composite [J]. *ACS Appl. Mater. Interfaces*, 2017, 9(22): 19176-19183.

[27] PARK K, VAIA R A. Synthesis of complex Au/Ag nanorods by controlled overgrowth [J]. *Adv. Mater.*, 2008, 20(20): 3882-3886.

[28] FANG G Q, JI Y N, XIAO Q, *et al*. Plasmonic Au@Ag-upconversion nanoparticle hybrids for NIR photodetection *via* an alternating self-assembly method [J]. *J. Mater. Chem.* C, 2022, 10(43): 16430-16438.

[29] LIN X, FANG G Q, LIU Y L, *et al*. Marangoni effect-driven transfer and compression at three-phase interfaces for highly reproducible nanoparticle monolayers [J]. *J. Phys. Chem. Lett.*, 2020, 11(9): 3573-3581.

[30] DONG J, GAO W, HAN Q Y, *et al*. Plasmon-enhanced upconversion photoluminescence: mechanism and application [J]. *Rev. Phys.*, 2019, 4: 100026.

[31] ZHUO X L, ZHU X Z, LI Q, *et al*. Gold nanobipyramid-directed growth of length-variable silver nanorods with multipolar plasmon resonances [J]. *ACS Nano*, 2015, 9(7): 7523-7535.

[32] CHOWDHURY S, JANA D. A theoretical review on electronic, magnetic and optical properties of silicene [J]. *Rep. Prog. Phys.*, 2016, 79(12): 126501.

[33] 洪锦泉, 郑标, 曾睿灵, 等. 多激发光窗口下银纳米颗粒表面等离激元增强多光子量子剪裁发光 [J]. 发光学报,

2022, 43(7): 1052-1060.
HONG J Q, ZHENG B, ZENG R L, *et al*. Multi-photon near-infrared quantum cutting enhancement by surface plasmon of Ag nanoparticles under multi-excitation [J]. *Chin. J. Lumin.*, 2022, 43(7): 1052-1060. (in Chinese)

[34] LUO X J, YUMINAMI R, SAKURAI T, *et al*. A novel synthesis method and up-conversion properties of hexagonal-phase $NaYF_4$:Er nano-crystals [J]. *J. Rare Earths*, 2013, 31(3): 267-270.

[35] YIN Z, LI H, XU W, *et al*. Local field modulation induced three-order upconversion enhancement: combining surface plasmon effect and photonic crystal effect [J]. *Adv. Mater.*, 2016, 28(13): 2518-2525.

[36] KIM J H, LIESS A, STOLTE M, *et al*. An efficient narrowband near-infrared at 1 040 nm organic photodetector realized by intermolecular charge transfer mediated coupling based on a squaraine dye [J]. *Adv. Mater.*, 2021, 33(26): 2100582.

[37] 季亚楠, 徐文. 稀土掺杂上转换纳米材料在近红外光电探测器中的应用 [J]. 硅酸盐学报, 2022, 50(12): 3185-3198.
JI Y N, XU W. Rare-earth element ions doped upconversion nanocrystals in near-infrared photodetectors applications [J]. *J. Chin. Ceram. Soc.*, 2022, 50(12): 3185-3198. (in Chinese)

周博明(2002-),男,湖南湘潭人,在读本科生,主要从事稀土掺杂上转换纳米颗粒的合成和光电探测器的制备。
E-mail: zhou111595505@163.com

季亚楠(1992-),女,辽宁大连人,博士,讲师,2020年于吉林大学获得博士学位,主要从事稀土纳米光电材料与器件的研究。
E-mail: jiyn@dlnu.edu.cn